Study of multipactor suppression of microwave components using perforated waveguide technology for space applications

Ming Ye, Yun Li, Yongning He, and Mojgan Daneshmand

Citation: Physics of Plasmas **24**, 052109 (2017);
View online: https://doi.org/10.1063/1.4982665
View Table of Contents: http://aip.scitation.org/toc/php/24/5
Published by the American Institute of Physics

Study of multipactor suppression of microwave components using perforated waveguide technology for space applications

Ming Ye,[1,2] Yun Li,[1] Yongning He,[1] and Mojgan Daneshmand[2]
[1]School of Microelectronics, Xi'an Jiaotong University, Xi'an 710049, China
[2]Department of Electrical and Computer Engineering, University of Alberta, Edmonton, Alberta T6G 1H9, Canada

(Received 25 February 2017; accepted 17 April 2017; published online 2 May 2017)

With the development of space technology, microwave components with increased power handling capability and reduced weight have been urgently required. In this work, the perforated waveguide technology is proposed to suppress the multipactor effect of high power microwave components. Meanwhile, this novel method has the advantage of reducing components' weight, which makes it to have great potential in space applications. The perforated part of the waveguide components can be seen as an electron absorber (namely, its total electron emission yield is zero) since most of the electrons impacting on this part will go out of the components. Based on thoroughly benchmarked numerical simulation procedures, we simulated an S band and an X band waveguide transformer to conceptually verify this idea. Both electron dynamic simulations and electrical loss simulations demonstrate that the perforation technology can improve the multipactor threshold at least ∼8 dB while maintaining the acceptable insertion loss level compared with its un-perforated components. We also found that the component with larger minimum gap is easier to achieve multipactor suppression. This effect is interpreted by a parallel plate waveguide model. What's more, to improve the multipactor threshold of the X band waveguide transformer with a minimum gap of ∼0.1 mm, we proposed a perforation structure with the slope edge and explained its mechanism. Future study will focus on further optimization of the perforation structure, size, and distribution to maximize the comprehensive performances of microwave components. *Published by AIP Publishing.*
[http://dx.doi.org/10.1063/1.4982665]

I. INTRODUCTION

Multipactor is an electron avalanching effect in a vacuum and high frequency environments, such as accelerators[1,2] and satellite payloads.[3–5] The occurrence of multipactor leads to many problems which are detrimental to system operation. Thus, a lot of work has been done to suppress this unwanted effect. For example, in Ref. 2, a magnetic field was used for this purpose. As regard to satellite applications, the weight of the components or subsystems is a critical specification and also a lot of work has been done on miniaturization of these components or subsystems.[4,5] From the weight point of view, the magnetic field method which will surely increase the components' weight may not be an optimal solution of multipactor suppression for satellite applications. Recently, surface treatment methods have been thoroughly studied for possible applications in multipactor suppression in high power microwave components of satellite systems. For example, in Refs. 6 and 7, the inner surfaces of components were roughened by selective or un-selective chemical etching, which results in micro/nanoporous structures. It has been shown both theoretically and experimentally in Refs. 8 and 9 that this kind of surface treatments can effectively reduce the total electron emission yield (TEEY), and thus, it is effective in multipactor suppression. The major challenges of this kind of methods may be the long term durability of the TEEY of micro/nanoporous surfaces and the increase in insertion loss.

With the development of fabrication technologies, especially the 3D printing technology, their impact on microwave applications has been increasing. Recently, a meshed waveguide structure fabricated by 3D printing technology was proposed for high power, low weight applications.[10] It was demonstrated that the meshed waveguide can effectively reduce the waveguide weight while keeping acceptable loss performance. In this work, we propose a multipactor suppression technology using similar perforated waveguide technology. The basic idea is that, when a microwave component is properly perforated, the perforation will behave as secondary electron absorbers and thus reduce the effective TEEY, which finally increases the multipactor threshold. So, this perforation technology is, as it were, similar to surface treatment methods. Compared with existing multipactor suppression technologies, the perforated waveguide method proposed here is capable of both increasing the power handling level and reducing the components' weight.

In Section II, we first conduct thoroughly the benchmarking of multipactor simulation and then present simulation results of both S band and X band waveguide transformers. In Section III, we discuss about the loss performance of perforated waveguide technology to further verify its applicability in real satellite applications. Conclusions are presented at last.

II. SIMULATION METHOD OF MULTIPACTOR AND VERIFICATION OF PERFORATION TECHNOLOGY

A. Benchmarking of multipactor numerical simulation

There are many codes for multipactor simulation,[11] to name a few, CST Particle Studio,[12–15] MSAT,[16] Spark3D,[14]

and MEST.[17] In this work, we use CST Particle Studio to evaluate the multipactor behavior. The basic simulation procedures include the following: first, the electromagnetic field distribution inside the simulated component is numerically calculated; then, initial electrons emitting from the predefined inner surface of the component are tracked using the law of Lorentz force; and third, secondary electrons are generated with the help of the probabilistic model of secondary electron emission in Ref. 18 when electron-wall interactions occur.

As presented in Ref. 15, it is not a trivial process to identify the multipactor occurrence from simulation results. Basically speaking, there are two diagnostics methods. The first method is based on the observation of the time evolution of the number of electrons. It can be said that multipactor occurred when an exponential increase in the electron number is observed or the electron number is multiplied by a predefined factor. However, the exponential factor or the multiply factor is somehow arbitrarily defined. An example of this strategy is presented in Appendix A. This electron number method is straight forward and has been widely adopted. However, when the input power is close to the multipactor threshold, the electron number will change slowly, and thus, it is a rather long time before the stop criterion is detected by the simulation program. In Fig. 1, we present an example of this method of multipactor diagnostics (we simulated a waveguide transformer). It can be seen that, when multipactor occurs at 50.75 dBm, the electron number grows exponentially.

The second multipactor diagnostics method is based on the average TEEY.[15] This quantity is defined as the ratio of the total number of emitted electrons from a predefined surface to the total number of electrons impacting on this surface. It was suggested that if this average TEEY is larger than 1, then multipactor occurs. In Fig. 2, we present this method of multipactor diagnostics using the same waveguide transformer as Fig. 1. It can be seen from Fig. 2(a) that, when multipactor occurs, the average TEEY periodically changes with its maximum exceeding 1.

Besides criterions for multipactor diagnostics, there are many simulation parameters which may affect the simulation results. For example, in Table I, we present the simulation results of a waveguide transformer (denoted as B-K-S9 in Appendix B) with various mesh numbers. It can be seen that,

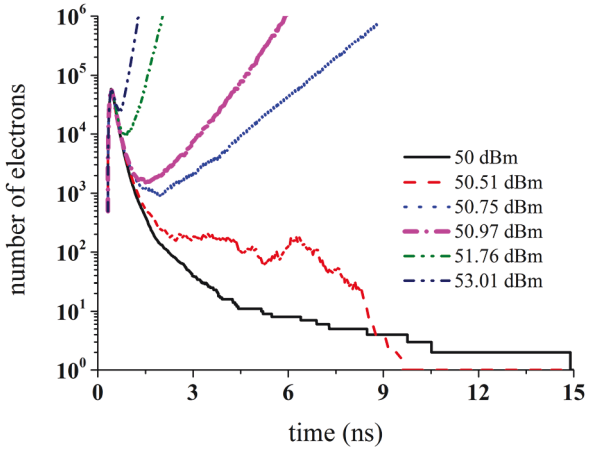

FIG. 1. Electron number evolution with time at various input powers.

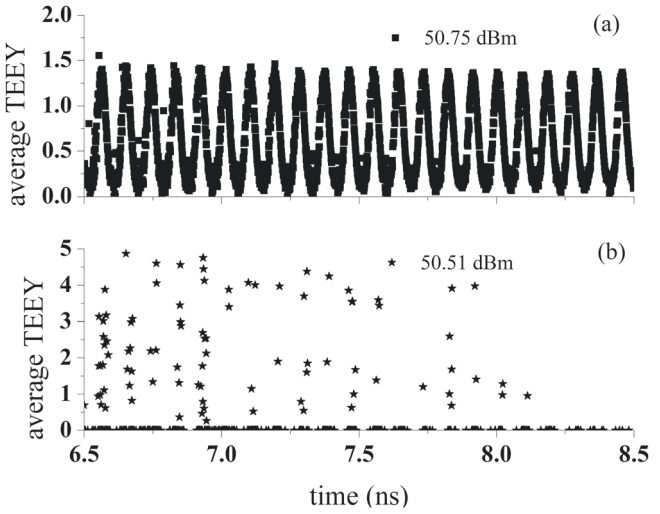

FIG. 2. Evolution of average TEEY when the input power is (a) equal to threshold and (b) below threshold.

when the mesh number reaches about 0.73×10^5, the threshold becomes converge to ~52.4 dBm. It should be noted that it would be better to check for the minimum proper mesh number for each simulated component.

The most important parameters for multipactor simulations should be the secondary electron emission parameters. Totally speaking, secondary electron emission properties include the total electron emission yield, electron emission energy distribution, and electron emission angle distribution. As presented in Refs. 11 and 14, the total electron yield has great effects on simulated multipactor threshold. In Refs. 19 and 20, it is demonstrated that the electron emission energy distribution can also affect the multipactor behavior. It should be noted that resonant and non-resonant components may depend on secondary electron emission properties in different ways. Based on these considerations, it would be clarity and necessary for one to define the secondary electron emission properties before presenting multipactor simulations. In this work, we used embedded silver data in CST which is from the ECSS standard.[11] The primary electron energy and incident angle dependence of TEEY are shown in Fig. 3(a). From Figs. 3(b)–3(d), the electron yield of true secondary electrons, rediffused electrons, and elastically backscattered electrons is shown, respectively. The secondary electron energy distributions at various incident primary electron energies are shown in Fig. 4. It should be noted that, for the silver surface, CST gives a much smaller backscattered peak in the energy distribution compared with data in Ref. 16. Anyway, multipactor predictions using this model agree well with experimental results.[11] In this work, all of the multipactor simulations are based on the secondary electron emission properties shown in Figs. 3 and 4.

At last, to benchmark our multipactor simulations, we simulated seven waveguide transformers and compared

TABLE I. Simulated threshold power with different numbers of cells.

Total number of cells (10^5)	0.25	0.73	1.5	3.9	8.1
Threshold power (dBm)	50.8	52.4	52.4	52.4	52.4

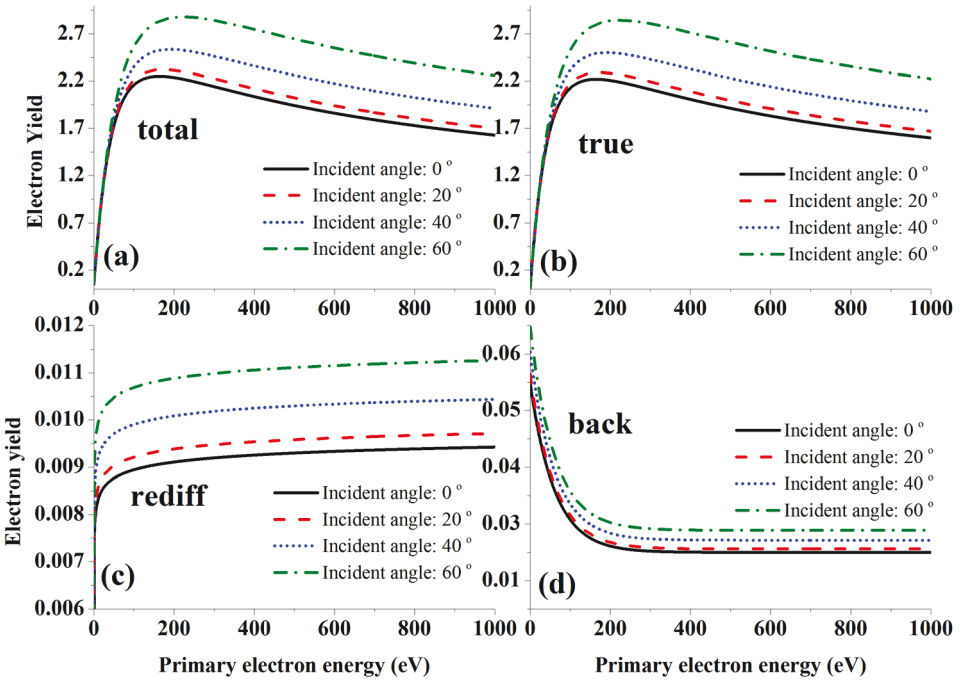

FIG. 3. Dependence on incident electron energy and angle of secondary electron emission yield of the silver surface used for multipactor simulations: (a) total yield, (b) true secondary electron yield, (c) rediffused electron yield, and (d) backscattered electron yield.

obtained simulation results with experimental results presented in literatures. One of these transformers works in the S band,[16] and others work in the X band.[11,21] The minimum gaps of these transformers range from ∼0.1 to 1.0 mm. It should be noted that, when dimension details are not available from the references (this is because the classical multipactor theory tells that it is the frequency and minimum gap determine that the threshold value), we designed and optimized the transformers ourselves, satisfying the requirements on minimum gap and working frequency. Details of transformer dimensions are presented in Appendix B. Both of the simulated and measured threshold dependences on the product of frequency and gap are shown in Fig. 5 (also given in Table IV of Appendix B). Totally speaking, the threshold deviations between simulations and measurements range from about 0.2 to 2.2 dB with an average of ∼1.1 dB. Considering the uncertainty introduced by transformer dimensions and measurements, these deviations are reasonably acceptable. Thus, the established multipactor simulation setups can be used to evaluate the multipactor behavior of perforated waveguide transformers.

In addition, we would like to mention that the product of frequency and gap is, to some degree, not enough to determine the multipactor threshold. To demonstrate this effect, we designed other 3 transformers with the same frequency and minimum gap with the transformer denoted as 'B-K-S10'. Details of the dimensions are also presented in Appendix B. The S-parameters of these 4 transformers are shown in Fig. 6, and their simulated thresholds are presented in Table II. It can be seen from Fig. 6 that all of the designed transformers have their return loss larger than 20 dB at the multipactor frequency point of 12.012 GHz. However, their working frequency bands are not the same. The transformer denoted as 'B-K-S10-1' has a much smaller frequency band. As shown in Table II, the maximum deviation of multipactor thresholds of these 4 transformers is 0.7 dB. Thus, this may be one of the reasons that our simulations deviate from literature

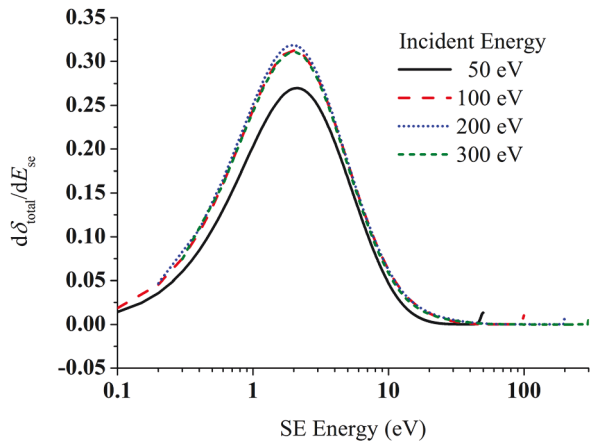

FIG. 4. Secondary electron emission energy distributions of the silver surface at various incident primary electron energies under normal incidence used for multipactor simulations.

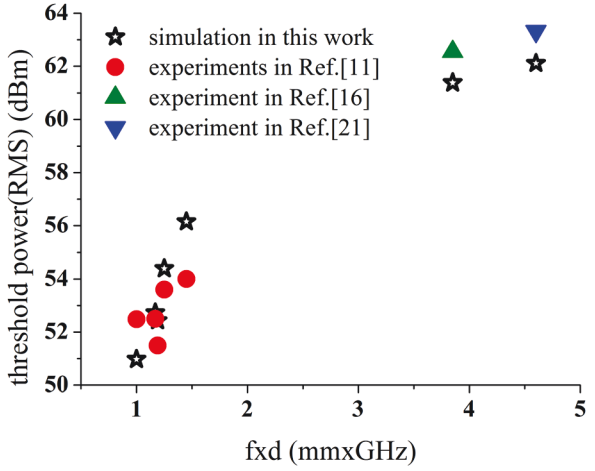

FIG. 5. Comparison between our multipactor threshold simulation results and experimental threshold results in literatures.

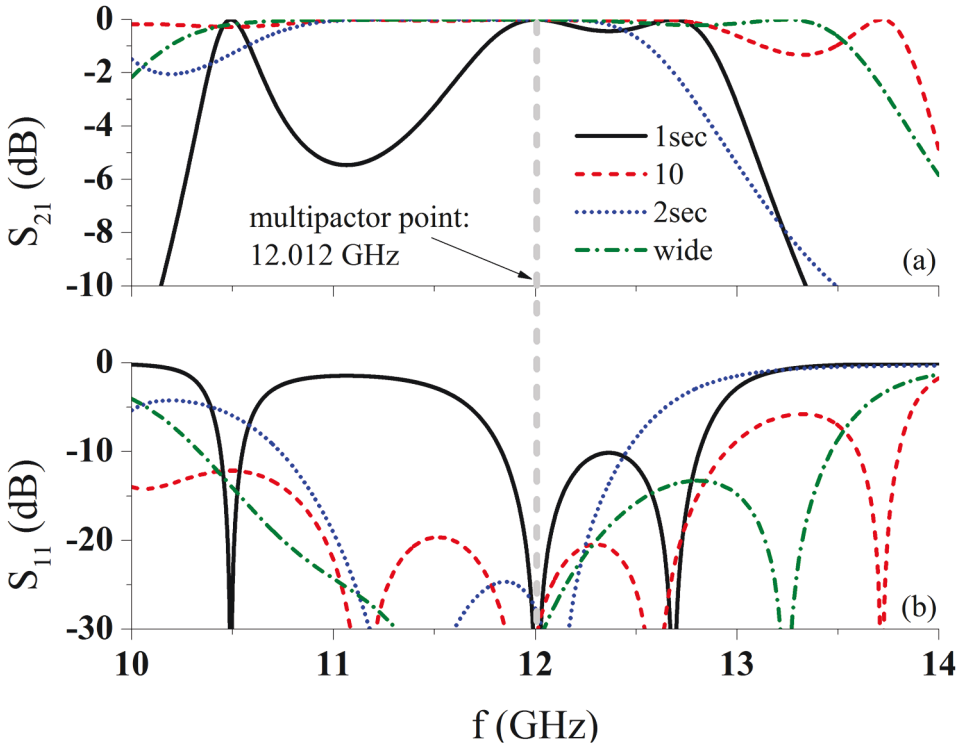

FIG. 6. S-parameters of transformers with the same product of frequency and minimum gap: (a) S_{21} and (b) S_{11}.

measurements to some degree. Another possible reason is that, as declared in Ref. 11, the ECSS silver TEEY data may deviate from real secondary electron properties.

B. Principle of multipactor suppression using the perforated waveguide

The principle of multipactor suppression using perforated waveguide technology is similar to the low TEEY surface modification methods to some degree as schematically shown in Fig. 7. As shown in Fig. 7(a), for a regular unperforated waveguide gap, all of the primary electrons impacting on the bottom wall can excite secondary electrons. When the bottom wall is perforated with periodical holes as shown in Fig. 7(b), part of the primary electrons will be incident to the holes and then go through them without generating any secondary electrons (strictly speaking, part of the primary electrons may impact on the lateral wall of the hole and thus excite secondary electrons; however, as a simplification, we can neglect these primary electrons to conceptually demonstrate the basic principle). Thus, when neglecting the possible effect of perforation on electromagnetic field distribution inside the waveguide gap, the perforated holes can be seen as electron absorbers as shown in Fig. 7(c). Here, electron absorbers can be ideally regarded as surfaces with a TEEY of zero for any primary electron energies. In other words, a perforated waveguide wall can be seen as a surface with non-uniform TEEY: the perforated part is of TEEY of zero, while the remaining part is of TEEY of regular metal materials. So, it could be expected that the perforation technology will be useful for multipactor suppression, and this idea will be verified through an established multipactor simulation model.

TABLE II. Simulated thresholds of transformers with the same product of frequency and gap.

Device#	B-K-S10-1	B-K-S10	B-K-S10-2	B-K-S10-w
Threshold (dBm)	52.4	52.7	52.9	53.1

C. Multipactor simulations of the S band waveguide transformer

In this section, we present multipactor simulation results of perforated S band waveguide transformers. The unperforated transformer denoted as "B-S-01" was used as reference, and its detail dimensions are given in Table V (for convenience, it is denoted as S-00 here). In this work, we simulated 3 perforated S band waveguide transformers with different perforation parameters as shown in Fig. 8, which are denoted as S-01, S-02, and S-03, respectively. From Figs. 8(a)–8(d), the inner surface of the reference and perforated transformers are shown and the size of the perforation area is described. For the transformer denoted as S-01, the total size of the perforation area is 37 by 51.4 mm^2 located at the center part of the transformer. The length of the perforated hole is 1.0 mm, and the gap between two adjacent holes is 0.2 mm which is shown in Fig. 8(f). Similarly, the total size of the perforation area of S-02 is 35.6 by 50 mm^2, and the hole length/gap is 2 mm and 0.4 mm, respectively. In other words, S-01 and S-02 have almost the same perforation area, but the perforated hole of S-02 is twice that of S-01. For the S-03 transformer, it is of the same hole size with S01, while its perforation area is expanded. In detail, the perforation area located at the center part is expanded to 51.4 by 51.4 mm^2, and what's more, two additional perforation areas (25 by 37 mm^2) are introduced close to the center perforation. A schematic view of the perforated S-03 transformer is shown in Fig. 8(e). It should be noted that, unlike the

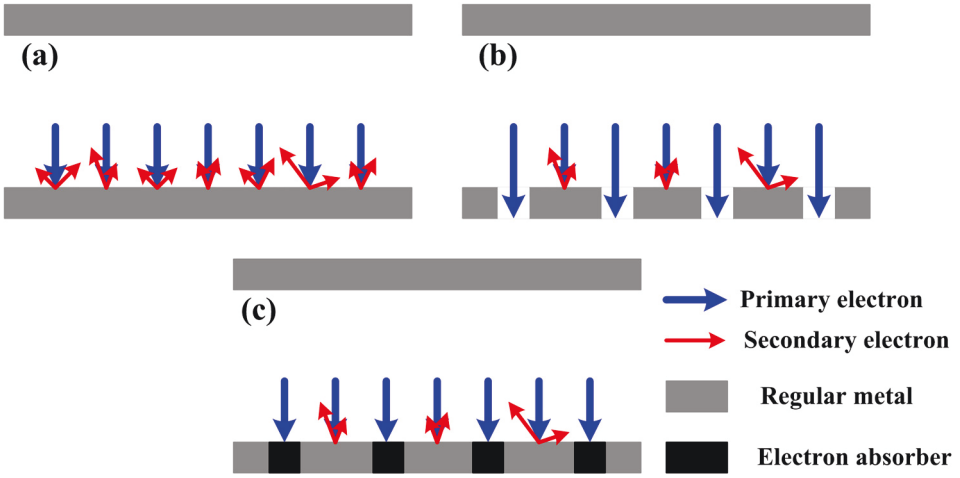

FIG. 7. Model of the perforated waveguide for multipactor suppression: (a) un-perforated case, (b) perforated case, and (c) electron absorber model for the perforated case.

perforated waveguide shown in Ref. 10 where the perforation was applied to the whole waveguide, we selectively perforated the top wall of the waveguide transformer based on the consideration of electrical performance (this will be discussed in more detail in Sec. II).

Multipactor simulation results of the perforated S band waveguide transformers are shown in Table III and Fig. 9. It can be seen from Table III that the multipactor threshold of the perforated transformer is improved from 3.7 to 7.6 dB compared with the reference transformer. The transformer S-03 has the highest threshold of 69.0 dBm, and the S-01 and S-02 transformers have almost the same threshold of ∼65 dBm. Thus, it is verified that the perforation technology is indeed useful to multipactor suppression. In Fig. 9(a), we show that the intensity of the electrical field inside the transformer helps with the interpretation of the multipactor simulation results. Since the red color indicates the high intensity of the electrical field, it can be seen that the strongest field locates at the center part of the transformer where perforation has been applied as shown in Fig. 8. From Figs. 9(b)–9(e), we show the electron distribution inside the waveguide transformers from which one knows where the multipactor will occur. For the S-00 transformer, the multipactor occurs at the edge of the center gap because the electric field intensity reaches its maximum there. For the perforated transformers, the multipactor occurs at different places. In fact, the multipactor occurs first at locations where a strong electric field exists. When perforation applied to the strongest field locations, the multipactor tends to occur at locations with the secondary strongest electric field. This tendency agrees well with the classical multipactor theory, and it provides a design degree of freedom. In other words, the most efficient way to suppress the multipactor is applying perforation to locations where a strong electric field exists.

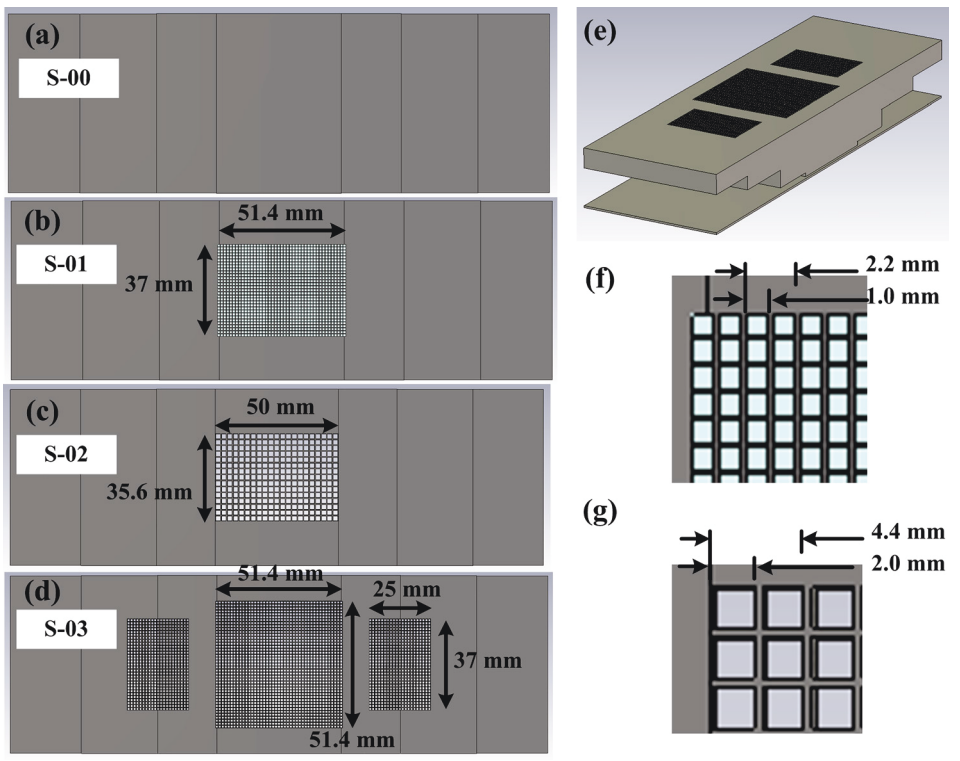

FIG. 8. Details of S band perforated waveguides for multipactor suppression: (a) un-perforated case, (b) perforated case 1 denoted as S-01, (c) perforated case 2 denoted as S-02, (d) perforated case 3 denoted as S-03, (e) full view of the perforated transformer of S-03 with the vacuum part neglected, (f) details of the hole size of S-01 and S-03, and (g) details of the hole size of S-02.

TABLE III. Simulated threshold power of the S-band perforated waveguide.

Device#	S-00	S-01	S-02	S-03
Threshold power (dBm)	61.4	65.1	65.4	69.0

D. Multipactor simulations of X band waveguide transformers

In this section, we apply perforation to the reference waveguide transformer denoted as B-K-S10 (for convenience, it is denoted as K-00). The multipactor occurring locations of this reference transformer are shown in Fig. 10(a), which are similar to those of the S-00 transformer. First of all, we applied perforation to the center 3 sections of K-00, which is denoted as K-01. The length of the perforated hole is 1.0 mm, and the gap between two adjacent holes is 0.2 mm (namely, the same with S-01). However, the multipactor occurs inside this perforated transformer when the applied power is 54.8 dBm, which is only a little higher than the reference power 52.7 dBm as shown in Fig. 10(b). So, it indicates that the perforation technology is not applicable in this case. However, when observing the electron distribution shown in Fig. 10(b), one could see that electron avalanche occurs at locations in-between adjacent holes. In fact, due to the rather small transformer gap (0.097 mm), the electrons

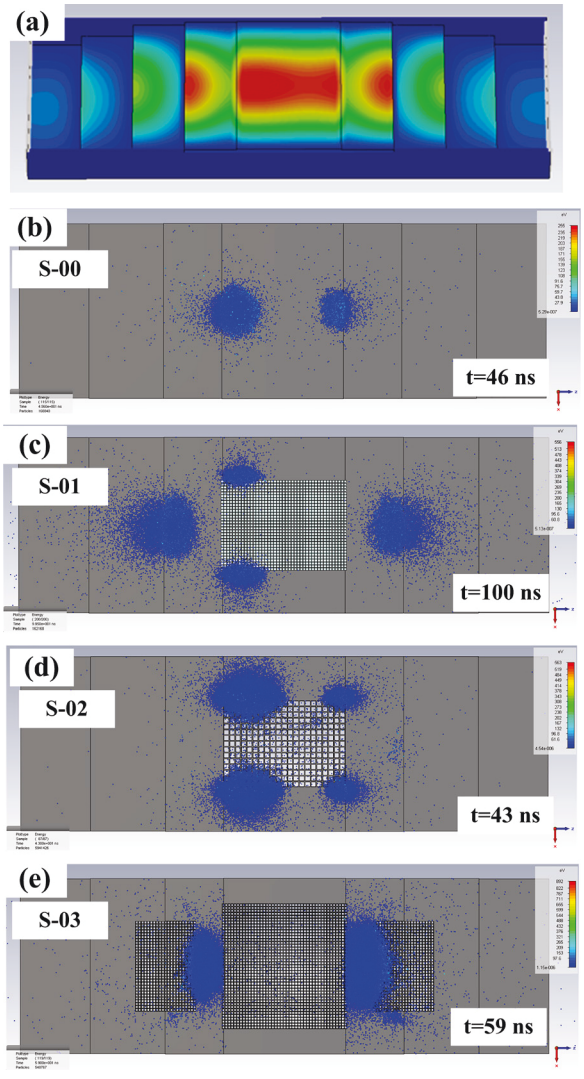

FIG. 9. Electric field distribution and electron space distribution inside reference and perforated waveguide transformers: (a) typical electric field distribution (red color indicates the strong field intensity) and electron space distribution with threshold power listed in Table III of (b) S-00 at 46 ns, (c) S-01 at 100 ns, (d) S-02 at 43 ns, and (e) S-03 at 59 ns.

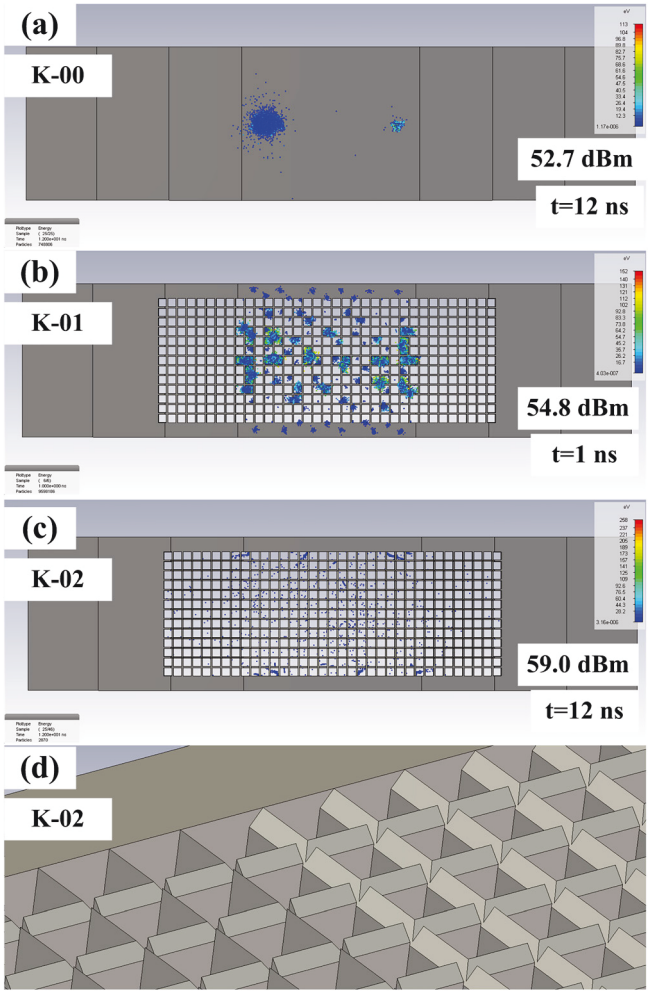

FIG. 10. X band perforated waveguide simulation results: (a) electron space distribution of K-00 with an input power of 52.7 dBm at 12 ns, (b) electron space distribution of K-01 with an input power of 54.8 dBm at 1 ns, (c) electron space distribution of K-02 with an input power of 59 dBm at 12 ns, and (d) 3D view of the slope edge perforation structure.

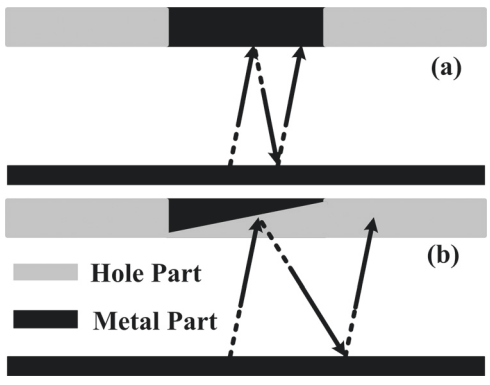

FIG. 11. Electron dynamics of (a) regular perforation and (b) slope edge perforation.

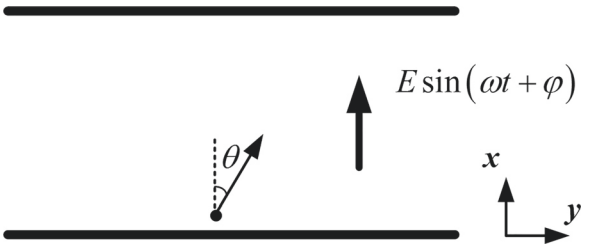

FIG. 12. Parallel plate waveguide model for multipactor analysis.

have rather small transverse displacement, and thus, they are not likely to go inside the perforated hole. This effect will be discussed quantitatively later. In order to guide the electrons go inside the perforated holes, we introduced the slope edge into the perforated holes as shown in Fig. 10(d). For this new perforation structure, we have simulated its multipactor behavior and observed remarkable improvement on threshold as shown in Fig. 10(c). The improvement of multipactor threshold in this case is at least 6.3 dB. The mechanism of multipactor improvement using this slope edge perforation is schematically shown in Fig. 11. For regular perforation as shown in Fig. 11(a), more flights are needed for electrons to obtain enough lateral displacement and then go inside the perforated hole. However, for the slope edge case as shown in Fig. 11(b), when electrons impacting on the slope edge, they will experience an obviously larger lateral displacement due to the cosine-like distribution of the emission angle of secondary electrons. In Ref. 22, this slope edge has also been adopted to guide electrons. Thus, this slope edge structure provides another degree of freedom when designing the perforation waveguide fit for suppressing the multipactor.

As mentioned above, the gap size has obvious effects on the multipactor suppression efficiency of perforated waveguides. To interpret this effect, we use the parallel plate waveguide model as shown in Fig. 12. With the excitation signal and coordination shown in Fig. 12, one can obtain the following electron trajectory equation:

$$x = x_0 + v_0 t + \frac{eE}{m\omega}\left[t\cos\varphi - \frac{1}{\omega}\sin(\omega t+\varphi) + \frac{1}{\omega}\sin\varphi\right]. \quad (1)$$

With this equation, we calculated the electron trajectory in both S band and X band cases. As shown in Fig. 13, for the S band case (the gap is 1 mm), the electron emitting from the

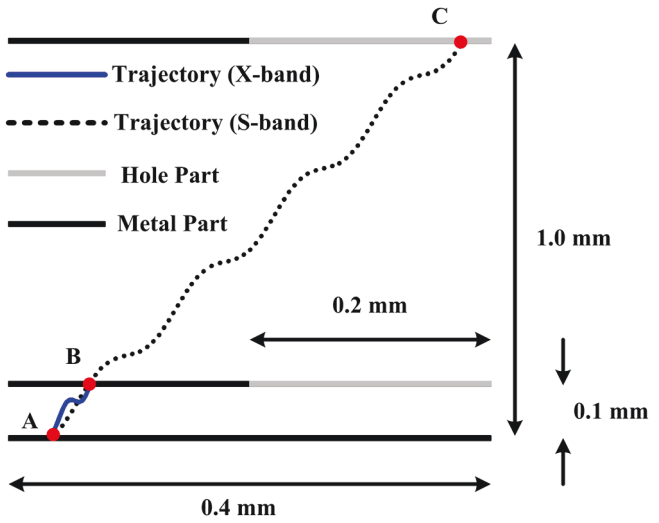

FIG. 13. Electron trajectory calculation results using Eq. (1). Calculation conditions: the emission polar angle is 20°, the emission energy is 2 eV, the input power is 400 W, the waveguide sizes are 19.05 mm × 0.1 mm and 72.14 mm × 1 mm, the working frequencies are 12.012 GHz and 3.85 GHz, and the emission phase is 80°.

bottom wall impacts with the top wall at point C while for the X band case (the gap is 0.1 mm) at point B. In other words, the secondary electron will be absorbed by the perforation hole only in the S band case. This observation agrees well with what we have observed above. In other words, from the multipactor suppression point of view, perforation technology is more applicable to components with larger minimum gap. For components with small minimum gap, the slope edge perforation technology as shown in Fig. 10(d) is recommended.

At last, we would like to introduce another degree of freedom which may be useful when designing perforation waveguides for multipactor suppression. In usual cases, the perforation holes are distributed uniformly and symmetrically on the waveguide surface such as in Ref. 10. However, one could also design asymmetrical perforations to improve the multipactor suppression. As shown in Fig. 14, one could introduce the two-side and asymmetrical perforation. Two-side perforation means more inner surface of the component will be of zero TEEY, and thus, a higher multipactor threshold can be obtained. Asymmetrical perforation means that the perforation holes on the top wall face to the un-perforated part of the

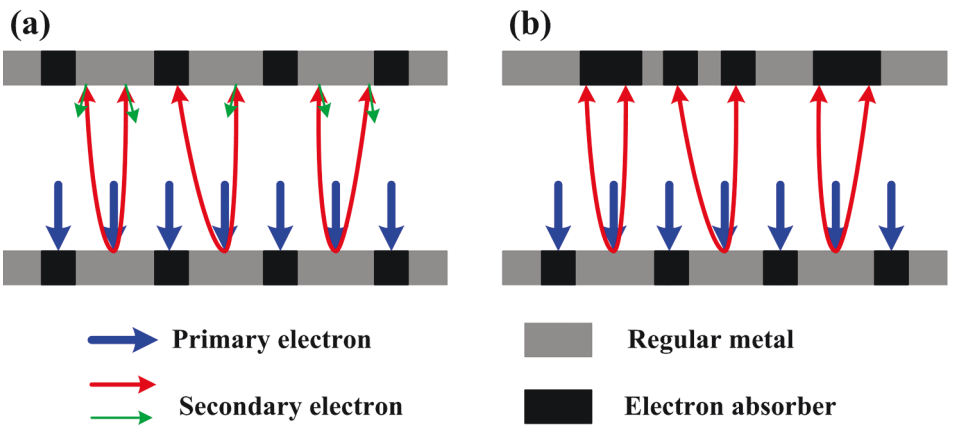

FIG. 14. Model of the two-side perforated waveguide for multipactor suppression: (a) symmetrical perforation and (b) asymmetrical perforation.

bottom wall (as shown in Fig. 14(b)). Compared with the symmetrical case (as shown in Fig. 14(a)), the perforation holes on the top wall can be designed at locations where electrons from the bottom wall impact. Thus, it could be expected that, even with small lateral displacement, the electrons are likely to go inside the perforation holes. In sum, with various degrees of freedom of perforation design, it is possible for one to obtain good trade-off among multipactor threshold, electrical/mechanical performance, and fabrication limitations.

III. ELECTRICAL PERFORMANCE CONSIDERATION

For satellite applications, it is always required that the loss of microwave components should be minimized due to the limited energy available on board. Thus, to further evaluate its applicability in practice, we simulated the electrical loss performance of the perforated waveguides. Physically speaking, the total loss of a perforated waveguide contains the following three: return loss, conductor loss, and radiation loss. Although the electrical loss performance of the perforated waveguide has been studied in Ref. 10, it tackled with regular waveguides with a much larger waveguide height than in this work. From our own simulations, we have found that, besides hole parameters, the electrical loss is also related to the height of the waveguide. We demonstrate the effect of the waveguide height on radiation loss using simulation results from WR-75 waveguides with the reduced height as shown in Fig. 15. To exclude the conductor loss, we have modeled the waveguide with perfect electric conductor (PEC) walls. When S-parameters are obtained from simulation, the radiation loss was calculated as follows:

$$\alpha_r = \frac{P_{in,dBm} - P_{trans,dBm}}{L_{wg}}\,\mathrm{dB/m} = \frac{10\log\left(1 - 10^{\frac{S_{11,dB}}{10}}\right) - S_{21,dB}}{L_{wg}}\,\mathrm{dB/m}. \quad (2)$$

Here, L_{wg} is the length of the waveguide. From both Figs. 15(a) and 15(b), we found that the waveguide with a smaller height will present a higher radiation. Besides, it can also be seen from Fig. 15 that a larger hole has obviously greater radiation than its counterpart. This tendency agrees with results in microwave shielding designs. So, a basic method for the improvement of possible radiation of the perforated waveguide is to reduce the hole size. One could also take the holes as evanescent waveguides due to their small transverse dimensions, and thus the radiation loss can also be minimized by increasing the waveguide wall thickness which is equivalent to increase the length of an evanescent waveguide. In other words, the waveguide thickness could be used as a degree of freedom when tackles with the radiation performance of perforated waveguides.

We examined the insertion loss of various transformers presented in Sec. III. The results are shown in Fig. 16.

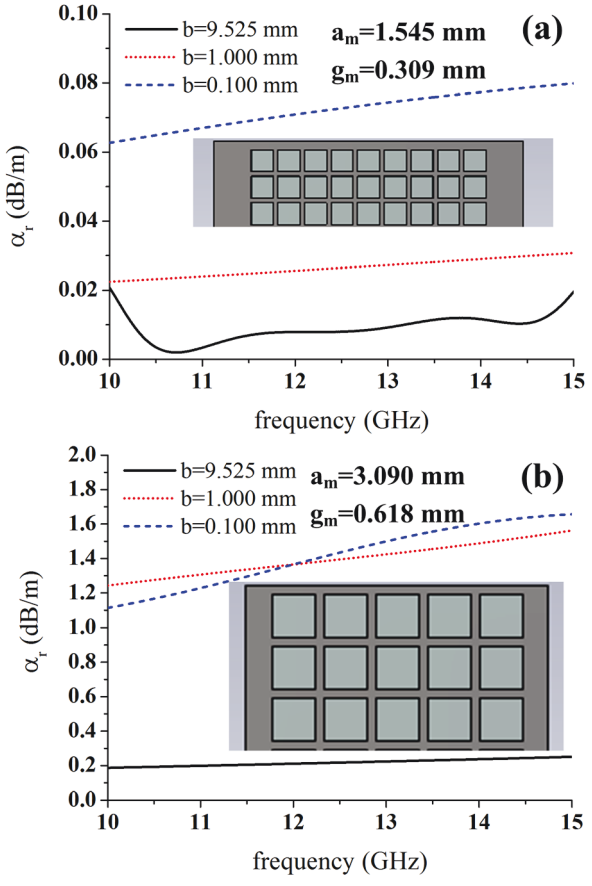

FIG. 15. Radiation loss dependence on the waveguide height of the perforated waveguide: (a) the length of the hole is 1.545 mm and the in-between gap is 0.309 mm and (b) the length of the hole is 3.09 mm and the in-between gap is 0.618 mm.

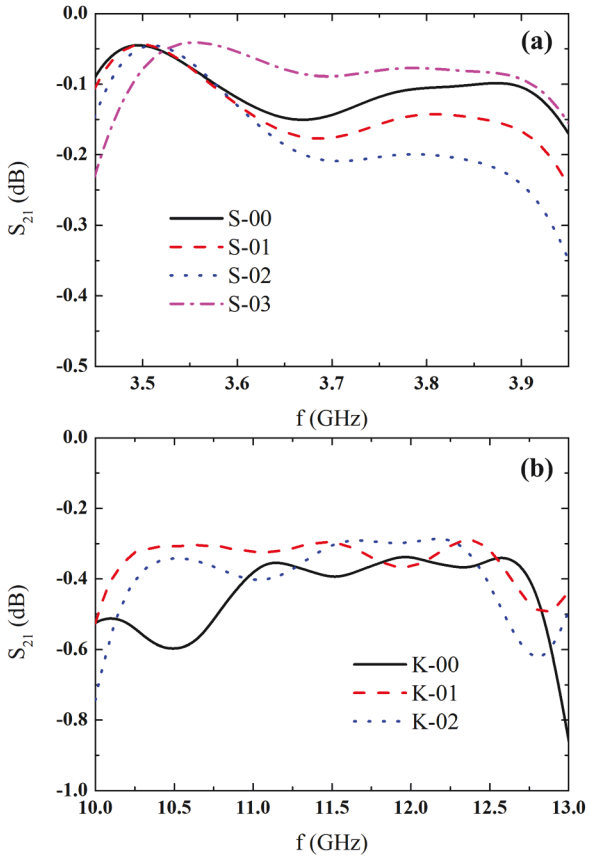

FIG. 16. Simulated S_{21} of perforated and reference waveguide transformers: (a) S band and (b) X band.

Totally speaking, the perforated waveguides have close insertion loss with their un-perforated counterparts. For the S band transformers, the insertion loss of S-02 is totally larger than that of the other transformers due to its larger hole size. For the X band transformers, the K-02 that presents the best multipactor suppression effect has roughly the same insertion loss with the reference transformer. So, it can be concluded that the properly designed perforated transformers are able to maintain their electrical loss performance while exhibiting obvious multipactor suppression effects. It is also possible to further optimize both the electrical loss performance and multipactor suppression performance through perforation design and optimization. With the development of fabrication technologies, especially the attracting 3D printing technology, this perforation technology has great potential in high power microwave industries.

IV. CONCLUSIONS

We proposed an efficient multipactor suppression technique using perforated waveguides. After fully benchmarked our multipactor simulations, we verified the perforation waveguide technology for multipactor suppression using S and X band waveguide transformers. The results of the S band transformers with a minimum gap of 1.0 mm show that a properly designed perforation can at least improve the multipactor threshold ~8 dB. For the X band transformers with a minimum gap ~0.1 mm, it was found that perforation with the slope edge is more efficient for multipactor suppression. We successfully used the parallel plate waveguide model to explain the gap size effect. We also simulated the electrical loss performance of perforated waveguide transformers. It was demonstrated that the perforated waveguide transformers maintain similar insertion loss with their un-perforated counterparts. So, it was fully verified that the proposed perforation technology has great potential in multipactor suppression for satellite applications. Further, considering the flexibility in perforation design such as perforation area/locations and perforation hole shape/size, the proposed perforation waveguide technology can be further designed and optimized to obtain optimal trade-offs between the multipactor performance and other specifics.

ACKNOWLEDGMENTS

This work was supported by the NNSFC (Grant No. 61501364) and China Scholarship Council.

APPENDIX A: EXPONENTIAL GROWTH OF THE ELECTRON NUMBER

Here, we give an example of exponential growth of the electron number when the multipactor occurs. A typical evolution of the electron number with time is shown in Fig. 17. The time interval T_a for observation is defined as 10 times of the signal period (signal frequency is 3.85 GHz). The start time of observation T_0 is set at the beginning of the 20th signal period. The number of observed time intervals is defined as 3. When the multipactor occurs, the electron number can be represented by $N = q\exp(pt)$. Here, q and p are fitting parameters and t represents time. Supposing that electron numbers at two successive time intervals t_1 and t_2 are N_1 and N_2, respectively, we have

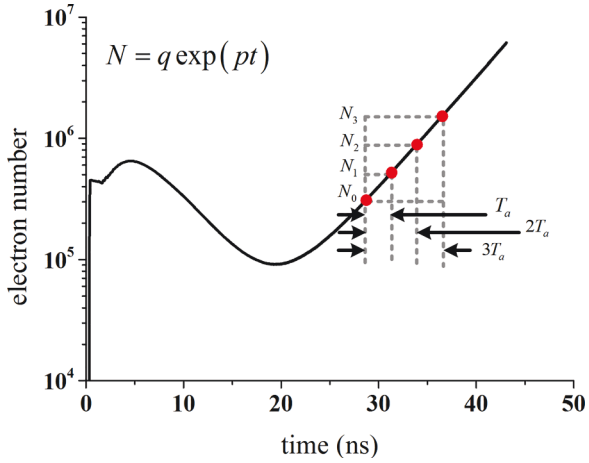

FIG. 17. Exponential growth of the electron number.

$$N_{t_2}/N_{t_1} = [q\exp(pt_2)]/[q\exp(pt_1)] = \exp[p(t_2 - t_1)] = \exp(pT_a). \quad \text{(A1)}$$

It can be seen that the parameter p determines the electron growth rate. As denoted in Fig. 17, supposing that the electron number at T_0, $T_0 + T_a$, $T_0 + 2T_a$, and $T_0 + 3T_a$ is N_0, N_1, N_2, and N_3, respectively, we can say the multipactor occurs only if $N_{i+1}/N_i \geq \exp(pT_a)$ for all $i = 0, 1, 2$. Otherwise, move T_0 forward one time interval and check the inequations again until the multipactor is detected or reaches the time end point. For the case shown in Fig. 17, when the exponential factor p is defined as 0.2, the multipactor can be detected. One could use this strategy to automatically stop the simulation once the multipactor is detected. This is helpful to improve the simulation efficiency. One ambiguous point may be that the exponential factor p is usually defined in a non-rigorous or an arbitrary manner.

APPENDIX B: INFORMATION OF WAVEGUIDE TRANSFORMERS USED FOR BENCHMARKING

In this appendix, we would like to present details on waveguide transformers used for benchmarking. This is because we found that, as it were, the minimum gap and

TABLE IV. Experimental and simulated threshold of waveguide transformers used for benchmarking.

Device#	Frequency (GHz)	Minimum gap (mm)	Experimental threshold (dBm)	Simulated threshold in this work (dBm)	Reference
B-S-01	3.85	1	62.6	61.4	16
B-X-01	11.5	0.4	63.3	62.1	21
B-K-S3	12.5	0.116	54.0	56.2	11
B-K-S4	11.095	0.09	52.5	51.0	11
B-K-S8	12.5	0.1	53.6	54.4	11
B-K-S9	11.095	0.107	51.5	52.4	11
B-K-S10	12.012	0.097	52.5	52.7	11

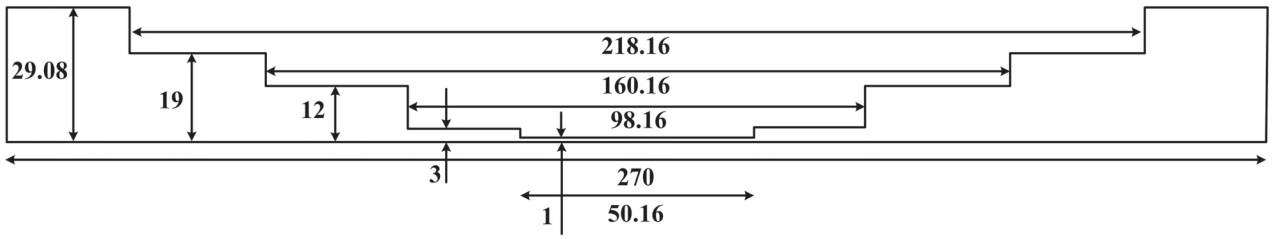

FIG. 18. Dimension of the S band waveguide transformer denoted as B-S-01 (the waveguide width is 72.14 mm).

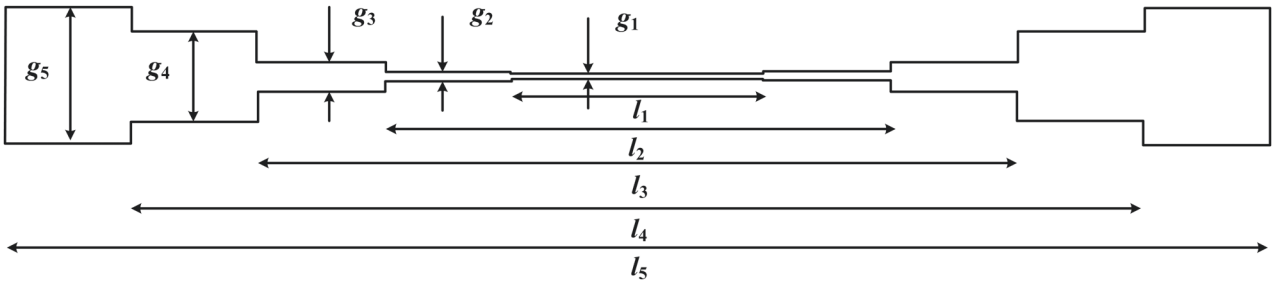

FIG. 19. Denotation of dimensions of X band waveguide transformers (the waveguide width is 19.05 mm).

TABLE V. Dimensions of X band waveguide transformers (the waveguide width is 19.05) (Unit: mm).

Device#	l_1	l_2	l_3	l_4	l_5	g_1	g_2	g_3	g_4	g_5
B-X-01	17.80	35.60	53.40	71.20	89.00	0.40	0.61	1.95	6.29	9.525
B-K-S3	20.87	38.51	55.76	74.30	96.17	0.116	0.189	1.009	4.785	9.525
B-K-S4	20.87	38.59	56.47	74.92	96.85	0.09	0.189	1.029	4.919	9.525
B-K-S8	21.99	40.11	57.97	75.59	96.24	0.1	0.205	1.043	4.699	9.525
B-K-S9	21.55	39.23	56.86	74.59	96.04	0.107	0.2	1.021	4.868	9.525
B-K-S10	22.02	40.08	57.99	75.56	96.26	0.097	0.205	1.044	4.695	9.525
B-K-S10-1	18.48	33.812	51.22	…	…	0.097	1.077	9.525	…	…
B-K-S10-2	14.53	32.04	48.34	66.06	…	0.097	0.31	3.03	9.525	…
B-K-S10-w	16.6	33.2	49.8	66.4	83	0.097	0.18	0.96	5.18	9.525

working frequency are not enough to fully characterize the multipactor behavior of microwave transformers. The transformers' denotation, working frequency, minimum gap, experimental threshold, simulated threshold, and according reference are presented in Table IV. It can be seen that the product of frequency and gap ranges from 1.0 to 4.6, and the working frequency covers both S and X bands. The difference between the simulated threshold of this work and experimental threshold in references ranges from 0.2 to 2.2 dB. The dimensions of the S band waveguide transformer are shown in Fig. 18, while the X band transformers are shown in Fig. 19 and Table V. As shown in Fig. 19, most of the X band transformers have 9 sections except following: B-K-S10-1 has only 5 sections and B-K-S10-2 has only 7 sections.

[1]C. Schlemper, M. Vogel, and X. Jiang, "Next generation of SRF-guns: low secondary electron yield based on a thin film approach," in Proceedings of SRF2015, Whistler, BC, Canada.
[2]C. Jing, S. H. Gold, R. Fischer, and W. Gai, "Complete multipactor suppression in an X-band dielectric-loaded accelerating structure," Appl. Phys. Lett. **108**, 193501 (2016).
[3]D. González-Iglesias, Á. Gómez, B. Gimeno, Ó. Fernández, A. Vegas, F. Casas, S. A. Hormigo, C. Vicente, J. Gil, R. Mata, I. Montero, V. E. Boria, and D. Raboso, "Analysis of multipactor RF breakdown in a waveguide containing a transversely magnetized ferrite," IEEE Trans. Electron Devices **63**(12), 4939–4947 (2016).
[4]O. A. Peverini, G. Addamo, R. Tascone, G. Virone, P. Cecchini, R. Mizzoni, F. Calignano, E. P. Ambrosio, D. Manfredi, and P. Fino, "Enhanced topology of E-plane resonators for high-power satellite applications," IEEE Trans. Microwave Theory Technol. **63**(10), 3361–3373 (2015).
[5]F. Teberio, I. Arregui, M. Guglielmi, A. Gomez-Torrent, P. Soto, M. A. G. Laso, and V. E. Boria, "Compact broadband waveguide diplexer for satellite applications," in IEEE MTT-S International Microwave Symposium (2016).
[6]W.-Z. Cui, Y. Li, J. Yang, T.-C. Hu, X.-B. Wang, R. Wang, N. Zhang, H.-T. Zhang, and Y.-N. He, "An efficient multipaction suppression method in microwave components for space application," Chin. Phys. B **25**(6), 068401 (2016).
[7]V. Nistor, L. A. González, L. Aguilera, I. Montero, L. Galán, U. Wochner, and D. Raboso, "Multipactor suppression by micro-structured gold/silver coatings for space applications," Appl. Surf. Sci. **315**, 445–453 (2014).
[8]M. Ye, Y. N. He, S. G. Hu, R. Wang, T. C. Hu, J. Yang, and W. Z. Cui, "Suppression of secondary electron yield by micro-porous array structure," J. Appl. Phys. **113**, 074904 (2013).
[9]Y. N. He, W. B. Peng, W. Z. Cui, M. Ye, X. L. Zhao, D. Wang, T. C. Hu, R. Wang, and Y. Li, "Thermal evaporated hyperbranched Ag nanostructure as an effective secondary-electron trapping surface coating," AIP Adv. **6**, 025122 (2016).
[10]E. A. Rojas-Nastrucci, J. Nussbaum, T. M. Weller, and N. B. Crane, "Meshed rectangular waveguide for high power, low loss and reduced weight applications," in 2016 IEEE MTT-S International Microwave Symposium.

[11]A. Al-Mudhafar, J. Puech, C. Miquel-Espanya, D. Raboso, H. Hartnagel, and EVEREST Consortium, "EVEREST simulation campaign results on multipactor effect using CST particle studio," in the 8th European Conference on Antennas and Propagation (2014).
[12]S. Lin, H. Wang, Y. Li, C. Liu, N. Zhang, W. Cui, and A. Neuber, "Multipactor threshold calculation of coaxial transmission lines in microwave applications with nonstationary statistical theory," Phys. Plasmas **22**, 082114 (2015).
[13]G. Burt and A. C. Dexter, "Prediction of multipactor in the iris region of RF deflecting mode cavities," Phys. Rev. Spec. Top.–Accelerators Beams **14**, 122002 (2011).
[14]N. Fil, M. Belhaj, J. Hillairet, and J. Puech, "Multipactor threshold sensitivity to total electron emission yield in small gap waveguide structure and TEEY models accuracy," Phys. Plasmas **23**, 123118 (2016).
[15]G. Burt, R. G. Carter, A. C. Dexter, B. Hall, J. D. A. Smith, and P. Goudket, "Benchmarking simulations of multipactor in rectangular waveguides using CST Particle Studio," in Proceedings of SRF2009, Berlin, Germany.
[16]Y. Li, W.-Z. Cui, and H.-G. Wang, "Simulation investigation of multipactor in metal components for space application with an improved secondary emission model," Phys. Plasmas **22**, 053108 (2015).
[17]J. de Lara, F. Pérez, M. Alfonseca, L. Galán, I. Montero, E. Román, and D. R. Garcia-Baquero, "Multipactor prediction for on-board spacecraft RF equipment with the MEST software tool," IEEE Trans. Plasma Sci. **34**(2), 476–484 (2006).
[18]M. A. Furman and M. T. F. Pivi, "Probabilistic model for the simulation of secondary electron emission," Phys. Rev. Spec. Top.–Accel. Beams **5**, 124404 (2002).
[19]H. Zhang, W. Cui, J. Li, Y. Li, and J. Yang, "Exploration of the relationship between emitted energy spectrum and multipactor threshold," in IEEE International Conference on High Voltage Engineering and Application (ICHVE) (2016).
[20]V. E. Semenov, E. I. Rakova, D. Andersona, M. Lisak, and J. Puech, "Multipactor in rectangular waveguides," Phys. Plasmas **14**, 033501 (2007).
[21]R. Wang, Y. Li, N. Zhang, W. Cui, M. Ye, and Y. He, "A novel method to improve the power capabilities of microwave components," in Proceedings of the 8th European Microwave Integrated Circuits Conference (2013).
[22]R. L. Geng, H. Padamsee, and V. Shemelin, "Multipacting in a rectangular waveguide," in Proceedings of the 2001 Particle Accelerator Conference, Chicago.